Quantitation in PET using isotopes emitting prompt single gammas: application to yttrium-86

Stéphan Walrand[1], François Jamar[1], Isabelle Mathieu[1], Joëlle Camps[1], Max Lonneux[1], Mérence Sibomana[2], Daniel Labar[2], Christian Michel[2], Stanislas Pauwels[1]

[1] Centre of Nuclear Medicine, University of Louvain Medical School, Avenue Hippocrate 54, 1200 Brussels, Belgium
[2] Laboratory of Positron Emission Tomography, University of Louvain Medical School, Louvain-la-Neuve, Belgium

Received: 23 July 2002 / Accepted: 27 October 2002 / Published online: 17 December 2002
© Springer-Verlag 2002

Abstract. Several yttrium-90 labelled somatostatin analogues are now available for cancer radiotherapy. After injection, a large amount of the compound is excreted via the urinary tract, while a variable part is trapped in the tumour(s), allowing the curative effect. Unfortunately, the compound may also be trapped in critical tissues such as kidney or bone marrow. As a consequence, a method for assessment of individual biodistribution and pharmacokinetics is required to predict the maximum dose that can be safely injected into patients. However, ^{90}Y, a pure β⁻particle emitter, cannot be used for quantitative imaging. Yttrium-86 is a positron emitter that allows imaging of tissue uptake using a PET camera. In addition to the positron, ^{86}Y also emits a multitude of prompt single γ-rays, leading to significant overestimation of uptake when using classical reconstruction methods. We propose a patient-dependent correction method based on sinogram tail fitting using an ^{86}Y point spread function library. When applied to abdominal phantom acquisition data, the proposed correction method significantly improved the accuracy of the quantification: the initial overestimation of background activity by 117% was reduced to 9%, while the initial error in respect of kidney uptake by 84% was reduced to 5%. In patient studies, the mean discrepancy between PET total body activity and the activity expected from urinary collections was reduced from 92% to 7%, showing the benefit of the proposed correction method.

Keywords: Yttrium-86 – Quantitation – Spurious coincidence – Somatostatin analogue

S. Walrand (✉)
Centre of Nuclear Medicine,
University of Louvain Medical School,
Avenue Hippocrate 54, 1200 Brussels, Belgium
e-mail: walrand@mnuc.ucl.ac.be
Tel.: +32-2-7642592, Fax: +32-2-7645408

Eur J Nucl Med (2003) 30:354–361
DOI 10.1007/s00259-002-1068-y

Introduction

Among the various radionuclides available for unsealed radiotherapy, yttrium-90 is one of the preferred isotopes. It is a pure high-energy β⁻particle emitter (end point energy: 2.27 MeV) with a half-life of 64.1 h. ^{90}Y is available in no-carrier-added concentration that allows preparation of a radioligand with high specific activity. Using a metal chelator, ^{90}Y can be complexed to monoclonal antibodies or peptide analogues. Among these radiopeptides, radiolabelled somatostatin analogues constitute a new group of promising therapeutic agents. ^{90}Y-DOTA-D -Phe^{1}-Tyr^{3}-octreotide (^{90}Y-DOTATOC), a Y-labelled somatostatin analogue, is currently under evaluation for the treatment of tumours expressing a high density of somatostatin receptors [1, 2, 3]. The first step in this evaluation is to quantitatively assess the biodistribution and pharmacokinetics of the compound in order to compute individual patient dosimetry data and the maximal dose that can be safely injected. However, ^{90}Y, being a pure β⁻particle emitter, cannot be used for quantitative imaging. Among the isotopes of yttrium emitting an in vivo detectable particle, only yttrium-86 has a half-life (14.74 h) long enough for this purpose [1, 2, 3, 4, 5, 6]. Furthermore, ^{86}Y has the interesting feature of being a β^+ emitter (33%), allowing the use of state of the art PET technology to study the whole-body distribution.

Unfortunately, ^{86}Y also emits 300% prompt single γ's per disintegration (Fig. 1) (β^+=33%, electron capture= 67%), the γ energies ranging between 0.139 and 4.9 MeV [7, 8, 9, 10]. After disintegration, the daughter nucleus (strontium-86) can be excited in about 30 different states, de-exciting to ground state by successive γ emission with a mean multiplicity of 6 [8, 9]. Of all the

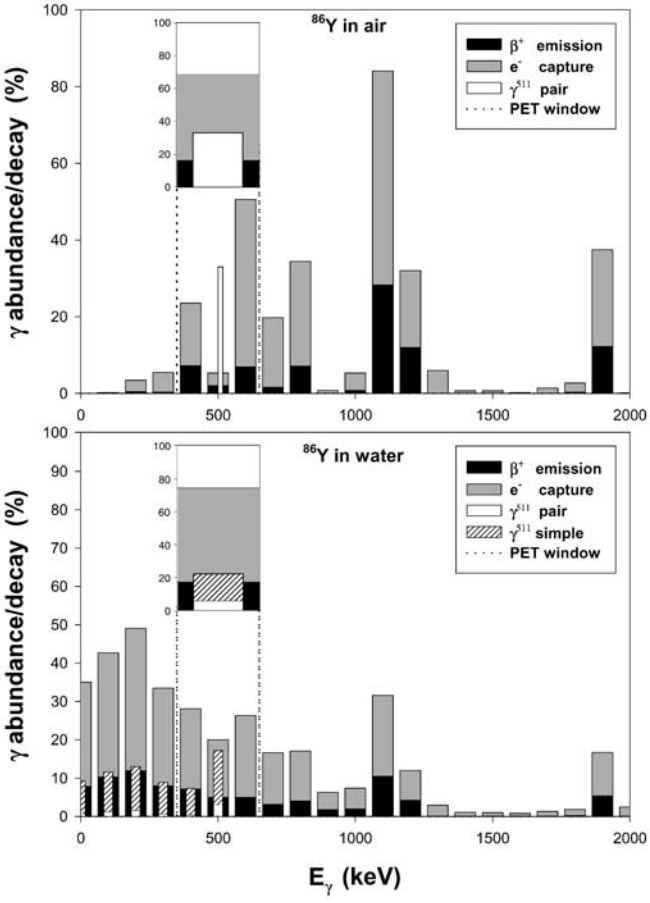

Fig. 1. γ-Ray abundance per decay for an ^{86}Y point source placed in air or surrounded by 15 cm water (data adapted from references [7, 8, 9, 10]). The spectrum was rebinned in a 100-keV histogram for clarity (^{86}Y emits 102 different γ-rays). Prompt single γ's emitted during β^+ emission are drawn in *black*. Note that after Compton scattering in water, the number of single γ's leaving the scatter medium during a β^+ emission becomes much higher than the number of γ^{511} pairs. Compton scattering in the PET shielding will further increase this effect. True coincidences can also occur between γ's emitted during an e^- capture. Spurious coincidences are much more probable in 3D mode, where non-coplanar γ's are accepted

γ-rays emitted during ^{86}Sr de-excitation, 25% have an energy within the PET acquisition energy window (typically 350–650 keV); a further 70% have an energy higher than 700 keV but, after Compton scattering in the patient or in the PET shielding, may also fall within the energy window. The magnitude of the process depends on the patient corpulence and on the activity distribution. Following the most probable decay path, 24.8% of ^{86}Y decays to ^{86}Sr3$^-$ (energy level of 2,997.35 keV) that subsequently may return to the ground state by emitting four γ-rays [9]. Of these four γ-rays, two may be directly detected (515.18 and 627.72 keV) while the other two (777.35 and 1,076.68 keV) may be detected after Compton scattering. These prompt single γ-rays hamper data acquisition by increasing the dead time random and multiple coincidences rate, especially in 3D mode [11]. However, the most disturbing effect with respect to quantification is the occurrence of true coincidences between either one single and a 511-keV or two prompt single γ-rays (referred to as spurious coincidences) during positron emission or electron capture. In both cases, these γ-rays do not have the 180° angular correlation and thus contribute to the background similarly to scattered (511-keV) radiation. Whatever acquisition mode is used in PET (2D or 3D), the spurious coincidences result in an overestimation of the true activity when not properly accounted for, and this error remains significant after classical scatter correction [12, 13, 14]. One should also note that modern scanners equipped with lossless coincidence processors no longer allow rejection of multiples (a large proportion of the spurious coincidence are probably multiples).

The sinogram tail fitting technique estimating the amount of activity outside the patient has been proposed to improve quantification [13, 14]. However, since this process is already used to normalise the 3D scatter sinogram estimated by Monte-Carlo simulation, it is hard to disentangle both effects in 3D. Moreover, the spatial distribution of the prompt single γ's and the scattered 511-keV γ's are not identical and do not behave in the same way when modifying the energy window. When data are acquired in 2D, the axial collimation of the septa improves the ratio between true positron and spurious coincidences. A correct way to approach the problem is a full Monte Carlo simulation using the prompt energy spectrum emitted from an ^{86}Y source with its various branchings and the source/scanner geometry.

After injection, variable amounts of ^{86}Y-DOTATOC are taken up by tumours expressing somatostatin receptors and a small percentage of the compound is retained by some normal tissues. As regards the kidneys and the red marrow, the two critical tissues as far as patient safety is concerned, the uptake ranges between 0% and 3% for kidneys and between 0% and 0.1% for a 12-cm-long segment of the spine red marrow. Since the effective half-life of ^{90}Y -DOTATOC in most organs exceeds 48 h, the measurements performed with the ^{86}Y-labelled surrogate should include delayed imaging up to 48 h post injection. Taking into account the physical half-life of ^{86}Y, the activity expected to remain at 48 h after injection of 370 MBq will not exceed 0.4 MBq in the field of view, and this will lead to a very low sinogram tail count rate. Also, in corpulent patients who almost fill the PET field of view, the sinogram tail may become very short or even disappear for some angular positions. In situations with such low statistics, line-by-line tail fitting becomes difficult and hazardous.

For estimation of spurious and scatter contribution (SSC) in whole-body data acquired in 2D,we propose an alternative method that is based on measured ^{86}Y point spread function (PSF) in an elliptical phantom simulating the abdomen. The SSC magnitude is derived from the total count number in the patient sinogram tail. The

correction method was first validated on phantom acquisitions and further applied to clinical studies performed in ten patients. The reconstructed whole-body activity was compared with the activity expected from urine collection counting.

Materials and methods

Data correction. The detected prompt coincidences can be true coincidences (TC), i.e. two γ's emitted during the same decay event involving a real simultaneous emission, or random coincidences (RC), i.e. two γ's produced by two independent decay events casually occurring within the PET time acceptance window (~20 ns). The true coincidences can be (1) usable coincidences (U_{511}), i.e. two 511-keV γ's emitted during the positron annihilation and thus travelling in opposite directions, (2) scattered coincidences (S_{511}), i.e. two γ's emitted during the positron annihilation, but with at least one of them undergoing Compton scattering and (3) spurious coincidences (SC), i.e. two γ's emitted during the same decay process, but with at least one of them deriving from the de-excitation of ^{86}Sr to ground state rather than from positron annihilation.

Figure 2 depicts the proposed scatter and spurious coincidences (SSC) subtraction method. The SSC contamination is treated like a perturbation. First, the random contamination is removed from the prompt coincidences by estimating the random coincidences using the classical delayed coincidences method. The estimation of true coincidences is further corrected for intrinsic efficiency by applying a dead time (function of bucket single rate) and a geometrical (solid angle) correction. These corrections are strictly valid for the U_{511} component and give the TC sinogram (Fig. 2). The TC sinogram is further reconstructed using the attenuation-weighted ordered subsets-expectation maximisation (OSEM) algorithm [15], generating a first estimated activity distribution A^0. Thereafter, the estimation of the SSC sinogram is calculated as follows:

$$\mathrm{SSC}(r,\phi,z) = \frac{\sum_{r,\phi}^{out(z)} \mathrm{TC}(r,\phi,z)}{\sum_{r,\phi}^{out(z)} (K \otimes A^0)(r,\phi,z)} \left(K \otimes A^0\right)(r,\phi,z) \qquad (1)$$

where z is the coordinate of the slice along the axial direction; r and ϕ are the radial and angular coordinates in the sinogram z; and $(K \otimes A^0)$ is the 3D convolution between the patient distribution activity A^0 and the PSF SSC library K (⊗, Fig. 2). The ratio before $(K \otimes A^0)$ in Eq. 1 is a normalisation factor (÷, Fig. 2). This normalisation ensures that for each sinogram z, the number of counts in the region corresponding to projection paths passing outside the patient is the same for the SSC estimation as for the TC sinogram. Indeed, in this region [*out(z)*in Eq. 1 and * in Fig. 2], all the coincidences detected are scatter or spurious coincidences (random coincidences are already removed). This region *out(z)*is chosen to be the area where the ratio between the blank scan and the patient's transmission scan is higher than 0.95.

The SSC non-stationary PSF library K was obtained once and for all by acquiring the prompt coincidences for an ^{86}Y point source successively placed in each grid hole drilled throughout a solid Plexiglas elliptical cylinder (Fig. 2). The U_{511} coincidences were removed from the true coincidences using the following procedure: for each line ϕ inside an interval of 2 cm width (6×PET σ) centred around the source location in the sinogram (Fig. 3), the pixel values were set to the mean value of the two pixels located at the limits of the interval. Note that these SSC PSFs also contain the S_{511} coincidences.

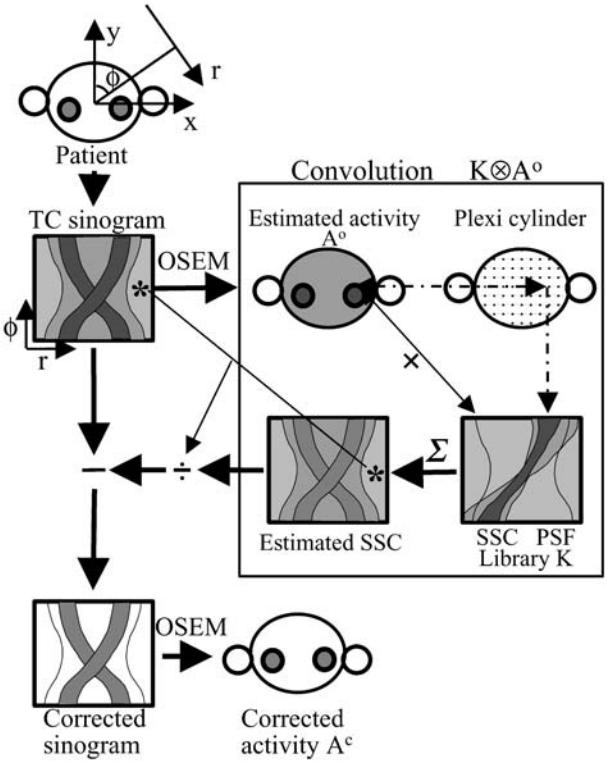

Fig. 2. Schematic representation of the scatter and spurious coincidences (SSC) subtraction process. For simplicity, transmission sinograms are not represented. The true coincidence (TC) sinogram is reconstructed using the attenuation-weighted OSEM algorithm. The resulting estimated activity A^0 is 3D convolved (⊗) with the SSC point spread function (PSF) library (K) as follows: (1) multiplication (×) of each activity pixel by the SSC PSF (K) obtained (– · – · →) from the point source located at the corresponding position (← · – · →) inside the Plexiglas cylinder, (2) summation (Σ) of the results computed for each pixel. The SSC estimation is further normalised (÷) to fit the total number of counts outside the patient (*) to the number of counts located outside the patient in the TC sinogram. The subtraction (–) of this estimated SSC from the TC sinogram provides a corrected sinogram, which, after reconstruction, generates the corrected activity distribution A^c. The same correction scheme can be iteratively applied using the last corrected activity distribution as a new starting estimated activity

The 3D convolution was obtained as follows:

$$\left(K \otimes A^0\right)(r,\phi,z) = \int dX dY dZ\, K\left(X, Y, r\frac{L(\phi)}{l(\phi,z)} - X_0(Z)\cos(\phi) - Y_0(Z)\sin(\phi), \phi, z - Z\right) A^0(X,Y,Z) \qquad (2)$$

where X and Y are the coordinates in the transverse plane and Z is the axial coordinate of the plane. $K(x, y, r, \phi, z)$ is the SSC coincidences contribution. K was measured from a point source located on a set of coordinates $(i \times h, j \times h, 0)$ forming a grid inside the Plexiglas cylinder (see "Materials and methods, SSC PSF library"). The needed value K on the coordinate (x,y) is obtained by a 2D linear interpolation from the four measured positions surrounding the point (x, y). $L(\phi)$ [or $l(\phi, z)$] is the width of the Plexiglas cylinder (or the width of the patient slice z) along the sino-

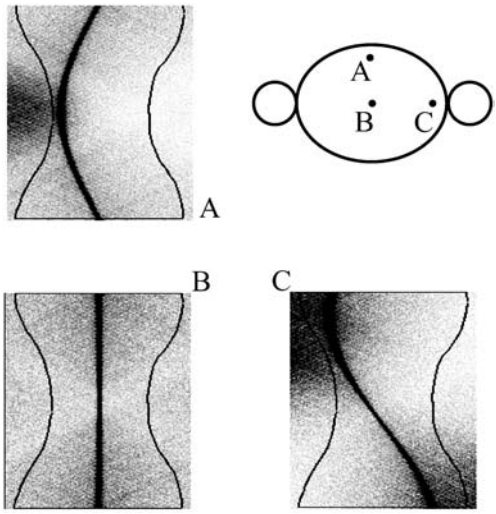

Fig. 3. True coincidences sinogram for a ^{86}Y point source located at the positions A, B and C inside the elliptical Plexiglas phantom used for determination of the PSF library. The phantom contour is drawn on the sinogram (*external curved lines*). Note that the amount and distribution of the scatter and spurious coincidences depend on the position of the point source in the phantom

gram radial coordinate r. This width is measured on the sinogram resulting from the ratio between the blank and the transmission sinogram using the same threshold of 0.95. The rescaling factor $\frac{L(\phi)}{l(\phi,z)}$ takes into account the difference between the patient and the Plexiglas cylinder widths. It is, of course, a rough approximation: changing the scatter medium size does not only correspond to a sinogram size scaling. $X_o(Z)$ and $Y_o(Z)$ are the transverse coordinates of the geometric centre of the patient slice Z. The shift coordinate factor $X_o(Z)\cos(\phi)+Y_o(Z)\sin(\phi)$ takes into account the fact that the patient is usually not accurately centred in the field of view of the camera.

The normalised estimated SSC is then subtracted (–, Fig. 2) from the true coincidences. Due to the very low count rate, the OSEM algorithm is used to reconstruct the data rather than the usual filtered back-projection. OSEM, like the expectation maximisation-maximum likelihood algorithm [16, 17], may be applied only to positive sinograms. This implies that the negative pixel values introduced by the subtraction of the estimated SSC, as a consequence of the statistical fluctuation, have to be removed. Setting these pixel values to 0 introduces a significant bias. The following correction was thus used to remove the negative pixel values in the subtracted sinogram: for each pixel $r\phi$ of sinogram z (beginning from z=0 to Nz) having a negative value $-p_z$ ($p_z>0$), the pixel value was set to 0 and $\min(p_z/2, p_{z-1})$ counts were removed from the pixel $r\phi$ of the sinogram $z-1$ and $p_z-\min(p_z/2, p_{z-1})$ counts were removed from the pixel $r\phi$ of the sinogram $z+1$. p_{z-1} is the value of the pixel $r\phi$ in the sinogram $z-1$. p_{z-1} is positive because the correction for negative values has already been done for the sinogram $z-1$ when correcting sinogram z.

The subtraction of the estimated SSC (Eq. 1) from the TC sinogram gives a corrected sinogram that, after reconstruction using the attenuation-weighted OSEM, will provide the corrected activity distribution A^c.

The same correction scheme can be applied iteratively using the last corrected activity distribution as a new starting estimated activity.

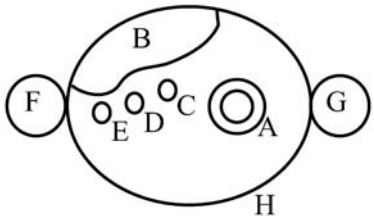

Fig. 4. Schematic representation of a transverse slice through the anatomical phantom simulating the abdomen and the arms: *A*, kidney; *B*, liver; *C–E*, tumours; *F, G*, arms; *H*, elliptical cylinder

Data acquisition. Acquisitions were performed using the Siemens ECAT Exact HR camera [18]. In order to minimise the SSC, acquisition of emission data was performed in 2D mode (septa extended) using a narrow energy window (411–611 keV). However, due to the complexity of the detector block setup and whole scanner normalisation, no other specific normalisation was performed than the one performed for the standard 350- to 650-keV energy window. Therefore, block corners would have a reduced efficiency. This effect was reduced by normalising the emission scans by the ratio between two daily blanks acquired with the two aforementioned energy windows. Furthermore, since an activity standard was acquired and reconstructed in the same way as for the patients, systematic biases were almost avoided. The azimuthal sampling was 196 angles with a pixel size of 1.65 mm. Transmission was performed using three rotating ^{68}Ge/^{68}Ga rod sources. Dead time and the random coincidences were corrected by the standard Siemens ECAT Exact HR procedure.

Standard. For each acquisition, phantom and patient, a standard source was acquired. The standard was a 0.3-ml aliquot of the injected solution contained in a 1-ml syringe enveloped in a 0.5-mm copper sheet in order to stop the positrons by annihilation. The standard and the injected dose activity were measured using a radioisotope calibrator following the manual procedure (CRC-12 Capintec, Pittsburgh, Pa., USA): calibration number set to 711, and displayed activity divided by 2.

SSC PSF library. A solid Plexiglas elliptical cylinder (40-cm long axis, 30 cm short axis and 12 cm length) similar in size to a standard human abdomen was perforated by 87 holes (5 mm diameter), forming a 2.5-cm mesh grid. The cylinder was positioned in the centre of the field of view (FOV) of the camera. Two circular cylinders (8 cm diameter and 12 cm length) filled with water were located at the right and left of, and in contact with, the elliptical cylinder to simulate the patient's arms. A 111-MBq ^{86}Y point source (size 3×3×3 mm) was placed in a hole of the phantom and a 20-min emission acquisition was performed. The source point was successively placed in each hole of one quadrant, and acquisitions were repeated. For the other three quadrants, PSFs were obtained by symmetry operation from the acquired data. Attenuation was estimated from a 1-h transmission scan performed on the Plexiglas cylinder without source.

Anatomical phantom. The anatomical phantom was made of an elliptical cylinder (30 cm long axis, 22 cm short axis and 20 cm length), filled with an active ^{86}Y-DTPA solution (4 mm) simulating the patient vascular and extracellular activity (background) (Fig. 4). To simulate the patient's arms, two circular cylinders (8 cm diameter and 10 cm length) filled with water were positioned at the right and left of the elliptical cylinder. A 1-l plastic

Table 1. Phantom compartment activities without and with (five iterations) SSC correction

Tissue	Volume (ml)	Activity (MBq)			Relative error %	
		True	No SSC correction	With SSC correction	No SSC correction	With SSC correction
Kidney cortex	100	2.29	4.22	2.41	+84	+5
Liver	1,000	10.36	14.47	9.73	+40	−6
Tumour C	8	2.18	2.29	1.96	+5	−10
Tumour D	8	4.14	4.49	4.04	+8	−10
Tumour E	8	9.14	10.36	9.79	+13	+7
Background	6,500	22.72	49.25	24.72	+117	+9
Arm F	500	0.00	0.71	0.02	n.a.	n.a.
Arm G	500	0.00	0.40	0.02	n.a.	n.a.

n.a., Not available

bag filled with an ^{86}Y solution simulated the liver. One kidney and its cortex were simulated by using two concentric cylinders (10 cm length), the inner cylinder (4 cm external diameter) being filled with water, while the external cylinder (6 cm internal diameter) was filled with an ^{86}Y solution. Three 1.3-cm-diameter vials, filled with an ^{86}Y solution, simulated tumour lesions. Table 1 details the compartment volumes and used ^{86}Y activities. The total acquisition time was 20 min. After 48-h decay, a 60-min transmission scan was acquired.

Patients. Ten patients with metastatic tumours expressing somatostatin receptors were studied. Whole-body emission and transmission scans were acquired over ten bed positions with overlap of seven planes (2.5 cm). Transmission scans, 5 min per bed position, were acquired prior to injection. The position of anatomical landmarks (eyes, nose, upper limit of the manubrium, navel and knees) was determined and noted using three orthogonal laser beams. Four hours after injection of 370 MBq ^{86}Y-DOTATOC, patients were carefully repositioned and a 50-min whole-body emission scan (10×5 min/bed position of 12.5 cm effective length) was performed. Urine was collected during the initial 4-h period following injection. The excreted fraction of the injected dose was determined by counting aliquots of the urine collection and a standard of the injected dose using a γ-counter (Wizard 3″ 1480, Wallac, Turku, Finland). Urine collection was incomplete for two patients, who were therefore excluded from the validation study. The study was approved by the Ethics Committee of the University of Louvain Medical School and all patients gave written informed consent.

Activity quantitation. Iterative reconstruction was performed in a 128×128 matrix (4.33 mm pixel size) using two iterations of weighted OSEM with 14 subsets of seven angles.

The acquisition of the standard was reconstructed using water and copper theoretical attenuation coefficients. The number of U_{511} coincidences was assumed to be the number of counts in a cylindrical volume of interest (VOI) (2 cm diameter and 3 cm length) drawn around the standard in the reconstructed activity map. Indeed, for a small source in air, Compton scattering is negligible. Thus, the S_{511} contribution was negligible and only 25% of the prompt single γ's, i.e. those with an energy within the acceptance window, contributed to spurious coincidences. Furthermore, due to their random emission angle, most SC-induced artefacts were outside the standard VOI.

Data acquired with the abdominal phantom and in patients were reconstructed with and without the SSC correction technique. In order to reduce the noise fluctuation due to the low count rate, a 3D gaussian filter of 1-cm full-width at half-maximum was applied on the final reconstruction. The SSC correction was limited to the first iteration for the patient studies. The phantom compartment activities and the tissue uptake in patients were computed using the number of counts in hand-drawn VOIs compared with the counts of the standard VOI.

Since the volumes of the tumours in the phantom were small (13 mm transverse diameter) and surrounded by background activity, the activity quantitation may have been affected by a partial volume effect due to the limited spatial resolution. To limit this effect, the tumour VOI was drawn large enough to include the whole tail of tumour activity. Cross-contamination from the surrounding background activity in this large VOI was further removed using:

$$A^{\text{tumour}} = A^{\text{VOI}} - \frac{V^{\text{VOI}} - 8}{6,500} A^{\text{bg}} \quad (3)$$

where A^{tumour} is the tumour activity, A^{VOI} is the activity of the tumour VOI and A^{bg} is the total background activity in the phantom. V^{VOI} is the volume of the tumour VOI in ml. Eight and 6,500 are the actual volumes (ml) of the tumours and of the background compartment. Eq. 3 was used for both uncorrected and SSC-corrected reconstruction.

86Y and 86Y-DOTATOC. Yttrium-86 was produced by irradiation of enriched ^{86}SrCO3 (Oak Ridge National Laboratory, Tenn.) following an ^{86}Sr(p, n)^{86} Y reaction as previously described [19]. The ^{86}Y formed is separated from Sr by co-precipitation with $LaCl_3$ in 25% aqueous ammonia and further purified on a cation-exchange column (Aminex-A5, Bio-Rad, Nazareth-Eke, Belgium) using hydroxy-isobutyric acid at increasing molarities (0.05–0.15 *M*). The elution solvent is evaporated to dryness and the recovered activity resuspended in 10 ml 0.02 *N* HCl. The radionucleidic purity was measured in an HPGe gamma spectrometer. Less than 1% ^{87}Y and 0.1% ^{88}Y were found in the preparations.

DOTATOC (Novartis Pharma AG, Basel, Switzerland and Mallinckrodt Medical, Petten, Holland) was available as a lyophilised kit containing 80 µg DOTATOC, 16 mg gentisic acid, 40 mg inositol and 80 mg ascorbic acid. For labelling, 1,110 MBq ^{86}YCl3 was added to a vial of DOTATOC and incubated at 100°C for 20 min.

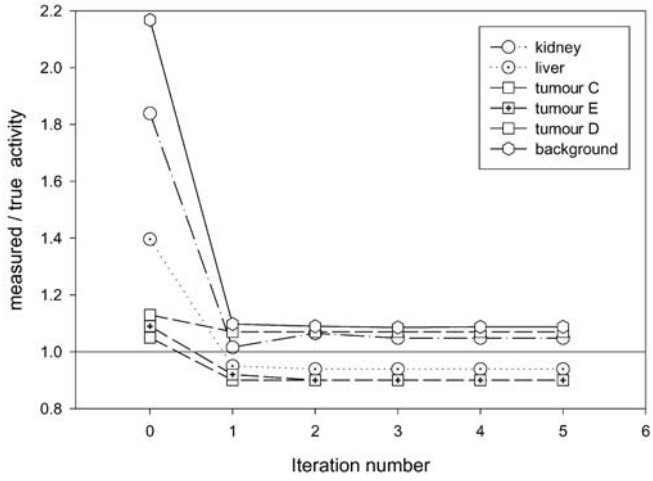

Fig. 5. Ratio between the computed and the true activities in the different compartments of the anatomical phantom as a function of the number of iterations in the SSC correction method. Iteration 0 corresponds to no correction. Note that after the first iteration, computed activities are already within 3% of the final value

Results

SSC PSF library

Figure 3 shows the acquired true coincidences sinograms for the ^{86}Y point source located in three different positions (A, B, C) inside the Plexiglas cylinder. The U_{511} coincidences were located along the sinusoidal curve passing through the pixels with the highest counts. The SSC profile strongly depended on the source position inside the cylinder, clearly showing the non-stationarity of the PSF. SSCs were also detected outside the cylinder boundaries.

Anatomical phantom

As shown in Fig. 5, the iterative process quickly converged. Indeed, after the first iteration all the compartment activities were already within 3% of their final value. SSCs were responsible for significant overestimation of activity, especially in the large area with low activity (up to 117% overestimation in the background compartment) (Table 1). Although the arm compartments did not contain any activity, SSC induced in these compartments major artefacts that were eliminated by the correction method. This artefactual activity was higher in the arm compartment close to the tumours (arm F in Fig. 4). The proposed SSC correction method reduced the relative overestimation from 84% to 5% for kidney cortex, from 40% to −6% for liver and from 117% to 9% for background.

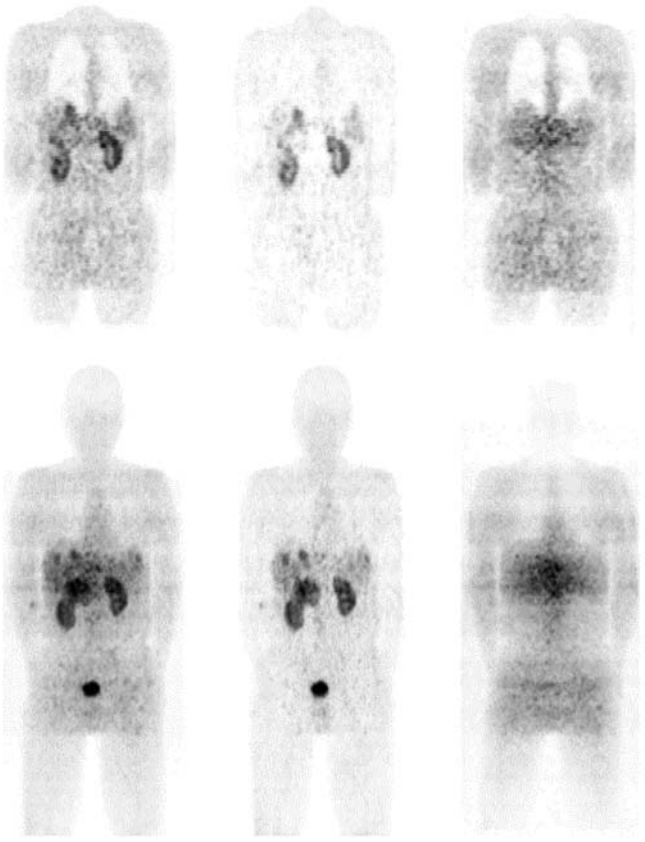

Fig. 6. PET study of a patient injected with 370 MBq ^{90}Y-DOTATOC (4 h p.i.): coronal slice passing through the kidneys (*top*) and projection of all coronal slices using the maximum pixel (*bottom*), without SSC correction (*left panel*) and with SSC correction (*middle panel*). The images on the *right* are the result of subtraction of the corrected from the uncorrected images. After SSC correction, the contrast is improved and the soft tissue activity is homogeneous. The artefactual activity present in the soft tissue around the bladder disappears after correction. The two images on the *right* clearly show that the counts reduction following SSC correction is not stationary

Patients

After injection of ^{86}Y-DOTATOC, 53±8% of the injected activity was recovered in the urine within 4 h p.i. Significant uptake was noted in tumours, in the kidney cortex and to a lesser degree in the liver and spleen. Figure 6 shows coronal views with and without SSC correction. Images without correction clearly showed strip artefacts around active tissues such as kidneys, bladder, spleen and tumours. These artefacts were significantly reduced by the SSC correction while the tumour-to-background contrast was enhanced. The soft tissue activity became homogeneous after the SSC correction. Without SSC correction, the whole-body activity was overestimated twofold (Table 2). With the SSC correction the residual relative error ranged from −12% to 21% with a mean value of 7%; there were underestimations in four cases,

Table 2. Patient whole-body activities with and without SSC correction. True activity is assumed to be the injected dose minus the activity in urine collections

Patient	Whole-body activity (% ID)			Relative error %	
	True	No SSC correction	With SSC correction	No SSC correction	With SCC correction
1	55.3	106.0	54.8	91	−1
2	43.2	82.0	37.8	89	−12
3	51.4	104.3	48.5	102	−5
4	34.2	60.7	34.5	77	1
5	37.3	80.5	45.2	115	21
6	46.2	84.5	47.2	82	2
7	51.1	96.1	54.3	88	6
8	56.7	110.4	53.1	94	−6
Mean	46.9	90.6	46.9	92	7

Table 3. Ratio between uncorrected and corrected tissue activities in patients

Patient	Whole body	Left kidney	Right kidney	Tumours
1	1.93	1.38	1.36	1.48
2	2.17	1.36	1.41	1.38
3	2.14	1.46	1.27	1.22
4	1.76	1.25	1.25	1.05
5	1.78	1.26	1.24	1.18
6	1.79	1.21	1.25	1.13
7	1.77	1.25	1.24	1.14
8	2.07	n.a.	n.a.	1.47

n.a., In patient no. 8, kidneys were not visualised

which shows that the systematic overestimation no longer persisted. Table 3 shows that the SSCs were responsible for an overestimation of kidney activity ranging from 21% to 46%, which might have resulted in inappropriate dose calculation. For tumours, the correction magnitude was even more variable, ranging from 5% to 48%.

Discussion

These phantom and patient studies demonstrate that prompt single γ's emitted by ^{86}Y are responsible for overestimations of activity that may reach 100% and 80% in the background and kidneys, respectively. Like scatter coincidences related to primary 511-keV γ's, spurious coincidences lead to misplaced disintegration events during the reconstruction process, i.e. a source located somewhere in the body induces artefactual activity in distant regions [12, 13, 14]. Contrast reduction and activity overestimation depend on the ratio between the tissue activity itself and the surrounding activity. This was clearly visible in patient studies (Fig. 6) and in the phantom study, where the overestimation for the arm close to the tumours was higher than that for the other one (Table 1). Similarly, for the same patient, SSC correction may lead to a reduction in counts that is different for the two kidneys depending on the proximity of activities. This demonstrates the non-stationarity of the SSC correction (Fig. 6, right panel).

Increase in patient corpulence led to a decrease in the number of U_{511} coincidences due to attenuation and to a minor increase in prompt single γ's within the energy window (Fig. 1). As a consequence, the ratio between U_{511} coincidences and spurious coincidences decreased when the patient width increased, which in turns explains the variation in the SSC correction of the whole-body activity. Although there was no obese patient in our study, the maximal whole-body activity overestimation could reach 100%. Activity distribution and patient shape are highly variable which explains why an individual correction method is required.

Our data show that the proposed SSC correction method quickly converges and can be stopped after the first iteration for patient studies, thereby reducing the noise magnification that would be induced by further iterations. This fast convergence results from the fact that the estimated SSC sinogram is normalised using the raw true sinogram. The SSC correction significantly improved the accuracy of quantitation: after correction the relative error of the whole-body activity ranged between −12% and 21% with a mean value of 7%. The balanced distribution of the relative error around 0 (four under- and four overestimations) shows that the systematic overestimation is well corrected.

It is worth noting that the present sorting hardware on the ECAT Exact HR (lossless coincidence processor) is not optimised for data acquisition of isotopes such as ^{86}Y, since all multiple events are stacked and sorted. For ideal positron isotopes (branching 100%, no prompt single γ-rays), the most probable multiple situation occurs when a γ-ray spreads its energy on neighbouring blocks. For isotopes such as ^{86}Y, multiple events occur more frequently when a coincidence event of two 511-keV γ's is detected together with a prompt single γ.

The prompt single γ's hamper data acquisition by increasing the dead time random and multiple coincidences rate, especially in 3D mode [11]. Depending on the

magnitude of this prompt single γ-ray component, it may saturate the scanner acquisition system more quickly than with pure positron emitters and the dead time correction algorithms may also diverge sooner due to a higher single's rate. Also, the amount of multiple coincidences will strongly depend on the activity outside the axial FOV owing to the very open geometry. The emission direction of prompt single or scatter γ's is randomly distributed; thus they rarely travel inside the same 2D transverse plane as a primary 511-keV γ. In 3D mode, the detection geometry is open, increasing the probability that unscattered or scattered prompt single γ's will be detected in coincidence with primary U_{511} γ's or with prompt single γ's. This will further increase the SSC contamination and may become uncorrectable for.

Future improvement of the method should include a spurious coincidence PSF that really takes into account the patient's size. Indeed, rescaling the PSF with the patient/Plexiglas cylinder size ratio may be considered as a rough approximation. This lack of accuracy is, however, compensated by the fact that the estimated spurious coincidences sinogram has only to have a good profile: the normalisation is achieved by using the property that prompt coincidences detected outside the patient are scatter or spurious ones. Another weakness of the proposed correction method is that the Plexiglas cylinder model does not take into account the heterogeneity of tissue density, which is especially significant in the chest. The accuracy of the proposed quantification has not been assessed for tumours located in the thorax. However, for critical organs located in the abdomen, such as kidneys, a homogeneous model should constitute an acceptable approximation. In the future, variables such as patient size and tissue density could be integrated in computation of spurious coincidences PSF by using Monte Carlo simulation rather than phantom data. It would also be worthwhile to evaluate the proposed method for correction of scatter coincidences in ^{18}F-FDG studies.

References

1. Forster GJ, Engelbach M, Brockmann J, Reber H, Buchholz HG, Macke HR, Rösch F, Herzog H, Bartenstein P. Preliminary data on biodistribution and dosimetry for therapy planning of somatostatin receptor positive tumours: comparison of Y-86-DOTATOC and In-111-DTPA-octreotide. Eur J Nucl Med 2001; 28:1743–1750.
2. Rösch F, Stolz B, Brockmann J, Köhle M, Muhlensiepen H, Marbach P, Herzog H, Muller-Gartner HW. Uptake kinetics of the somatostatin receptor ligand [86Y]DOTA- d -Phe1-Tyr3-octreotide (86Y-SMT487) using positron emission tomography in non-human primates and calculation of radiation doses of the 90Y-labelled analogue. Eur J Nucl Med 1999; 26: 358–366.
3. De Jong M, Valkema R, Jamar F, Kvols LK, Kwekkeboom DJ, Breeman WA, Bakker WH, Smith C, Pauwels S, Krenning EP. Somatostatin receptor-targeted radionuclide therapy of tumors: preclinical and clinical findings. Semin Nucl Med 2002; 32: 133–140.
4. Herzog H, Stöcklin G, Lueders C, Qaim SM, Rösch F, Feinendegen LE. Measurement of pharmacokinetics of yttrium-86 radiopharmaceuticals with PET and radiation dose calculation of analogous yttrium-90 radiotherapeutics. J Nucl Med 1993; 34:2222–2226.
5. Rösch F, Plag C, Neumaier B, Braun U, Müller-Gärtner HW, Herzog H, Stöcklin G. Radiation dose of yttrium-90 citrate and yttrium-90 EDTMP as determined via analogous yttrium-86 complexes and positron emission tomography. Eur J Nucl Med 1996; 23:958-966.
6. Wester HJ, Rösch F, Herzog H, Smith-Jones P, Stolz B, Bruns C, Brockmann J, Stöcklin G. PET-pharmacokinetics off 18F-octreotide: a comparison with 67Ga-DFO- and 86Y-DTPA-octreotide. Nucl Med Biol 1997; 24:275–286.
7. Erdtmann G, Soyka W. Die γ-Linien der Radionuklide Band 1. KFA Julich September 1973.
8. King MM. Nuclear data sheet 1997; 80:567.
9. Firestone RB, Baglin CM, Chu FS, Shirley VS, Zipkin J. In: Shirley V, ed. Table of isotopes.New York: Wiley-Interscience; 1996:510–512.
10. Pagani M, Stone-Elander S, Larsson SA. Alternative positron emission tomography with non-conventional positron emitters: effects of their physical properties on image quality and potential clinical applications. Eur J Nucl Med 1997; 24:1301–1327.
11. Martin CC, Satter MR, Nickerson LDH, Christian BT, Nickles RJ. Quantitative PET with positron emitters that emit prompt gamma rays. IEEE Trans Med Imag 1995; 14:681–687.
12. Pentlow KS, Larson SM, Erdi YE, Finn RD, Humm JL. Phantom measurements to investigate the use of yttrium-86 and PET to determine the in vivo distribution of yttrium-90 labelled pharmaceuticals. J Nucl Med 1998; 39:791–791.
13. Pentlow KS, Larson SM, Erdi YE, Finn RD, Humm JL. Effects of cascade gamma rays in PET imaging quantitation. J Nucl Med 1999; 40:1238–1238.
14. Kohlmyer SG, Shoner SC, Lewellen TK, Miyaoka RS, Eary JF. Quantitative accuracy of PET imaging with yttrium-86. J Nucl Med 1999; 40:1237.
15. Hudson HM, Larkin RS. Accelerated image reconstruction using ordered subsets of projection data. IEEE Trans Med Imaging 1994; 13:601–609.
16. Shepp LA, Vardi Y. Maximum likelihood reconstruction for emission tomography. IEEE Trans Med Imaging 1982; 2:113–122.
17. Lange K, Carson R. EM reconstruction algorithms for emission and transmission tomography. J Comput Assist Tomogr 1984; 8:306–316.
18. Wienhard K, Eriksson L, Michel C, Bruckbauer T, Pietrzyk, Dahlbom M, Heiss WD. The ECAT EXACT HR: performance of a new high resolution positron scanner. J Comput Assist Tomogr 1994; 18:110–118.
19. Rösch F, Qaim SM, Stöcklin G. Production of the positron emitting radioisotope 86Y for nuclear medical applications. Int J Appl Radiat Isot 1993; 44:677–681.